Advanced Ceramics Progress: Vol. 11, No. 3, (Summer 2025) 24-30

Materials and Energy Research Center
MERC

Contents lists available at ACERP

Advanced Ceramics Progress

Journal Homepage: www.acerp.ir

Original Research Article

Photocatalythic Activity of ZnO-WO_3 for Methyl Orange Degradation

Reza Irankhah [a]*, Ali Balooch [b], Hassan Koohestani [c]

[a] *Assistant Professor, Department of Ceramic, Faculty of Materials and Metallurgical Engineering, Semnan University, Semnan, Iran.*
[b] *MS Student, Faculty of Materials and Metallurgical Engineering, Semnan University, Semnan, Iran.*
[c] *Associate Professor, Faculty of Materials and Metallurgical Engineering, Semnan University, Semnan, Iran.*

* Corresponding Author Email: R.Irankhah@semnan.ac.ir (R. Irankhah)
URL: https://www.acerp.ir/article_243082.html

ARTICLE INFO

Article History:
Received 13 November 2025
Received in revised form 14 February 2026
Accepted 24 April 2026

Keywords:
ZnO,
WO_3,
Photocatalysis,
Green Synthesis,
Methyl Orange

ABSTRACT

The elimination of dyes via photocatalysis is a promising approach for achieving pollution-free environments. ZnO, WO3, and ZnO–WO3 (in a 1:1 weight percentage ratio) were synthesized through a green synthesis method. The resulting products were characterized using X-ray diffraction (XRD), Fourier transform infrared spectroscopy (FTIR), field emission scanning electron microscopy (FESEM), energy dispersive spectroscopy (EDS), and diffuse reflectance spectroscopy (DRS). The XRD pattern indicates the formation of crystalline structures of ZnO, WO3, and ZnO–WO3. Optical studies revealed that the optical band gaps for pure ZnO, pure WO3, and the ZnO–WO3 photocatalysts were 4.20 eV, 3.03 eV, and 3.29 eV, respectively. The photocatalytic activity of the synthesized samples was evaluated through the degradation of methyl orange (MO). The obtained results demonstrated that the synergistic effect between WO3 and ZnO contributes to enhanced charge separation and a reduction in the recombination rates of charge carriers, thereby significantly improving photocatalytic performance. It was observed that 100% degradation of the MO dye can be achieved by the ZnO/WO3 composite after 15 minutes of visible light irradiation.

https://doi.org/10.30501/acp.2026.556425.1187

1. INTRODUCTION

Zinc oxide (ZnO) has been extensively studied as a photocatalyst owing to its chemical stablity, low toxity, affordability, and promising photocatalytic characteristics. However, its relatively large band gap restricts its absorption primilary to the UV light region (Faris et al., 2023; Lam et al., 2013). The band gap of ZnO is approximately 3.37 eV, which limits the effective harvesting of visible photons and consequently diminishes its photocatalytic efficiency under visible light irradiation (Lam et al., 2013). Unfortunately, ZnO is prone to rapid recombination of photogenerated electron–hole pairs during the photocatalytic process (Zheng et al., 2009). A highly effective approach to overcome these limitations is to create heterojunctions by combining ZnO with another semiconductor. In the literature, ZnO paired with various metal oxides such as SnO_2, Fe_2O_3, TiO_2, and CuO (Hamrouni et al., 2013; Liu et al., 2008; Moradi et al., 2016; Pei & Leung, 2011; Saravanan et al., 2013; Yan et al., 2011) with the resulting composites typically exhibit superior performance compared to pristine ZnO. Among these options, tungsten trioxide (WO_3), which has a narrower band gap (~2.7 eV), demonstrates significant responsiveness to visible light and is therefore regarded as a promising candidate for constructing ZnO-based heterostructures (Mohammed et al., 2022). Although sevral studies have been published on ZnO-WO_3 composites (Adhikari et al., 2015; Alam et al., 2024; Chaudhary et al., 2020; E et al., 2019; Hunge et al., 2018; Lam et al., 2013; Xie et al., 2014; Xu & Chen, 2023; Yu et al., 2011; Zhang et al., 2022), the photocatalytic performance of green-synthesized ZnO–WO_3 composites specifically for the degradation of methyl orange under

Please cite this article as: Irankhah, R. Balooch, A. & Koohestani, H. (2025). Photocatalythic Activity of ZnO-WO_3 for Methyl Orange Degradation. *Advanced Ceramics Progress*, *11*(3), 24-30. https://doi.org/10.30501/acp.2026.556425.1187

visible irradiation remains inadequately reported. Therefore, the present work focused on the green synthesis of pure WO_3, pure ZnO, and a ZnO–WO3 composite and assessed their photocatalytic efficacy for the removal of methyl orange in an aqueous environment.

2. MATERIALS AND METHODS

Zn(NO3)2·6H2O (98.5%) and WO3 (99%) were used as sources of zinc and tungsten, respectively. Ammonia solution was used as a pH-adjusting agent. Methyl orange dye was obtained from DRM Laboratory. To prepare the saffron petal extract, 10 g of saffron petals were macerated in 100 mL of distilled water using an ultrasonic bath. The prepared mixture was boiled for 2 h, then filtered and centrifuged for 10 min. The precipitation method was employed for the preparation of the ZnO–WO_3 photocatalyst. First, a certain amount of WO3 was ultrasonically dispersed in 50 mL of the extract. Subsequently, a certain amount of Zn(NO3)2·6H2O was ultrasonically dissolved in the solution. The solution was then treated with ammonia until the pH reached 10. The as-formed precipitates were washed with distilled water, dried at 60 °C, and finally calcined at 450 °C for 2 h. ZnO–WO_3 composites with weight ratios of ZnO to WO3 of 100:0, 50:50, and 0:100 were synthesized. The obtained materials were labeled as 100ZnO, 50WO_3-50ZnO, and 100WO_3, respectively. Figure 1 displays the green synthesis of the ZnO–WO_3 composite using saffron petal extract.

XRD data and phase evaluation were collected using a diffractometer (Bruker D8) with Cu-Kα radiation. The morphology of the samples was determined using field emission scanning electron microscopy (CIQTEK-EM5000X). Meanwhile, energy dispersive X-ray analysis (EDX) was also used to determine the elemental composition on the surface of the photocatalysts. Fourier transform infrared (FTIR) spectra were recorded using a PerkinElmer instrument. UV–Vis diffuse reflectance spectra (DRS) were recorded on an S4100 SCINCO spectrophotometer in the wavelength range of 200–900 nm to investigate the optical absorption properties and determine the band gap energy. The photocatalytic activity of the synthesized samples was evaluated for the treatment of 50 mL of methyl orange (MO) dye in aqueous solution with an initial concentration of 100 ppm, using 0.1 g of the synthesized powders. The photocatalytic tests were performed in a Pyrex batch reactor with a 500 W fluorescent lamp as the light source. Samples were withdrawn from the solution at intervals of 5, 15, and 30 min, and the degradation efficiency was calculated.

3. RESULTS AND DISCUSSION

3.1. XRD study

The X-ray diffraction patterns of pure ZnO, pure WO_3, and the 50WO_3-50ZnO composite are shown in Figure 2.

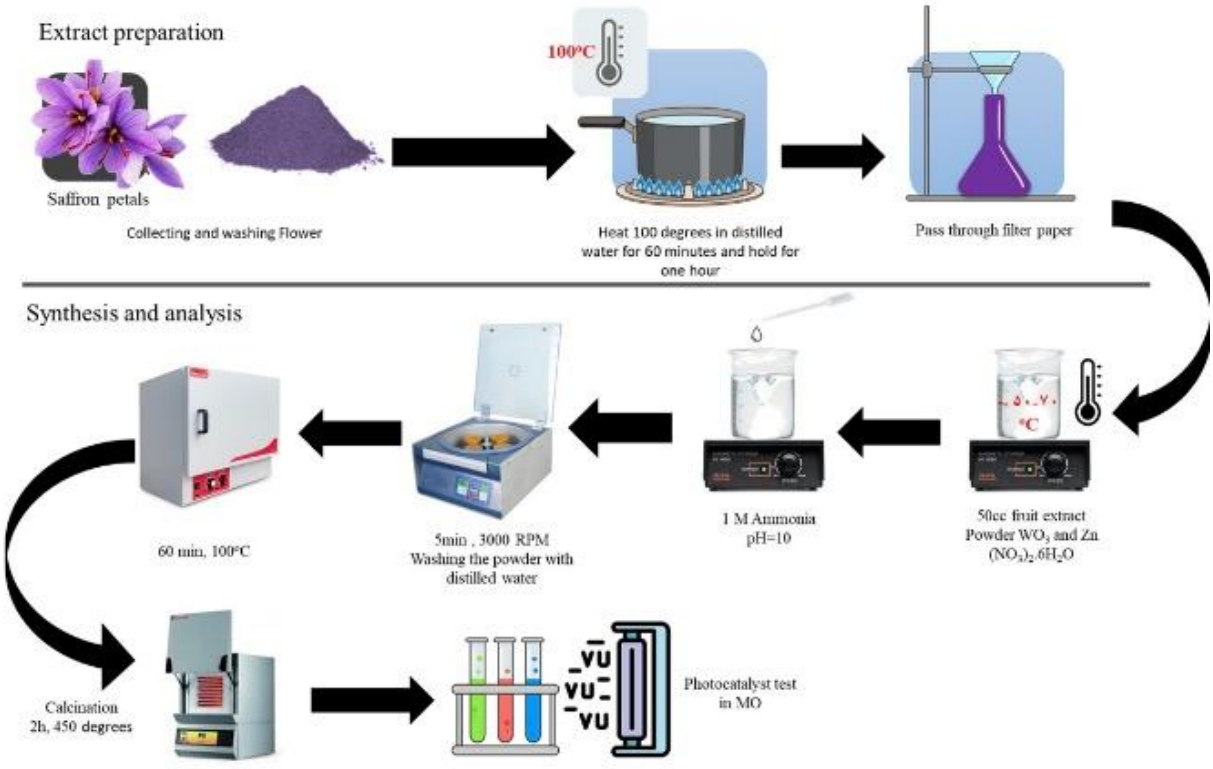

Figure 1. Schematic diagram of synthesis of ZnO - WO_3 composite using saffron petal extract.

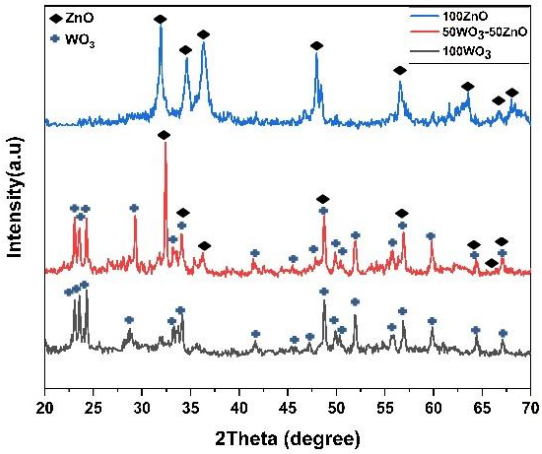

Figure 2. XRD of synthesized (a) 100ZnO, (b) 100WO_3, and (c) 50WO_3-50ZnO composite.

The XRD spectra obtained from the synthesized ZnO reveal diffraction peaks at 2θ = 34.57, 35.46, 36.29, 48.46, 56.59, 63.57, 66.65, and 67.90, indicative of a typical hexagonal crystal structure (JCPDS card No. 00-01-1136). The diffraction peaks of WO_3 can be accurately indexed to the monoclinic phase of WO3 (JCPDS card No. 00-002-0308). Moreover, the XRD spectra of the 50WO3-50ZnO composite exhibit both WO_3 and ZnO peaks. The XRD analysis did not reveal any characteristic peaks corresponding to impurities. The crystallite size (D) of the samples was determined through X-ray line broadening using Scherrer's formula ($D = 0.9\lambda/\beta\cos\theta$), where D represents the average crystallite size, λ = 1.5418 Å is the wavelength of the CuKα line, β denotes the FWHM of the respective peak, and θ signifies Bragg's diffraction angle. The mean crystallite sizes of the 100ZnO and 100WO_3 samples, calculated from the most intense peaks, were found to be 30 and 50 nm, respectively. Furthermore, the mean crystallite sizes of the ZnO and WO_3 phases in the 50WO3-50ZnO sample were determined to be 17 and 30 nm, respectively. A reduction in crystallite size correlates with an increase in specific surface area, which in turn enhances the photocatalytic degradation rate (Nandiyanto et al., 2017).

3.2. Morphological study

The morphological features of pure ZnO, pure WO_3, and the 50WO_3-50ZnO composite were analyzed using field emission scanning electron microscopy (FESEM). Figure 3 illustrates the surface morphology of the as-synthesized photocatalysts. Pure ZnO powder (Figure 3a) exhibited a uniform cauliflower-like structure, whereas pure WO_3 displayed nanosheets with a thickness of approximately 40 nm (Figure 3b). The cauliflower particles were measured to be around 150 nm, with clusters of nanoparticles within the cauliflower ranging from 15 to 30 nm. The particles in the 50WO_3-50ZnO sample (Figure 3c) are well dispersed and interconnected. Furthermore, the morphologies of WO3 and ZnO nanoparticles did not show significant alterations compared to the pure samples.

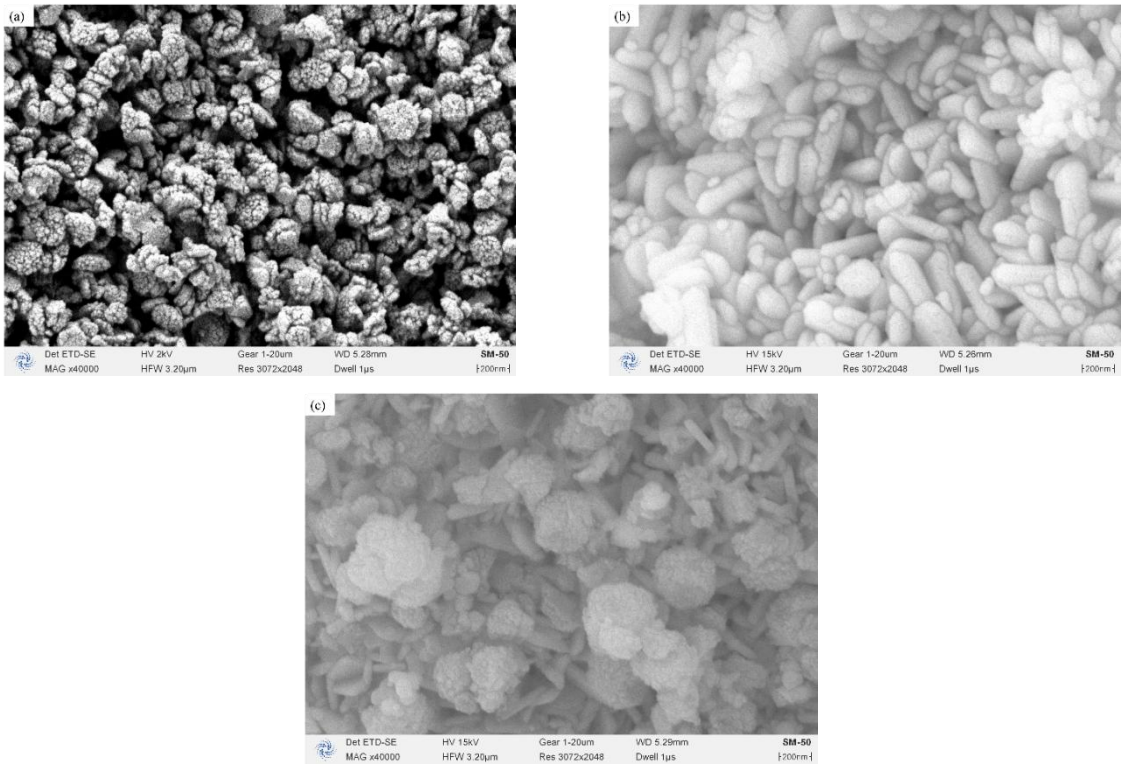

Figure 3. FESEM micrograph of the (a) 100ZnO, (b) 100WO_3, and (c) 50WO_3-50ZnO samples.

The spatial composition of the as-synthesized photocatalysts was examined using energy-dispersive spectroscopy (EDS). Figure 4 presents the EDS spectra of the 100ZnO, 100WO_3, and 50WO_3-50ZnO photocatalysts. As shown, the presence of W, O, and Zn elements was observed. In addition, the minor peaks of C and Au are attributed to the carbon resin and conductive coating, respectively. In the EDS spectrum of 100ZnO, only peaks corresponding to Zn and O were detected. Conversely, W peaks were also identified in the 50WO3-50ZnO photocatalyst. The atomic percentages of Zn and W in the 50WO3-50ZnO nanocomposite were found to be 28.51% and 53.41%, respectively. The EDS results validate the successful synthesis of the ZnO–WO_3 composite.

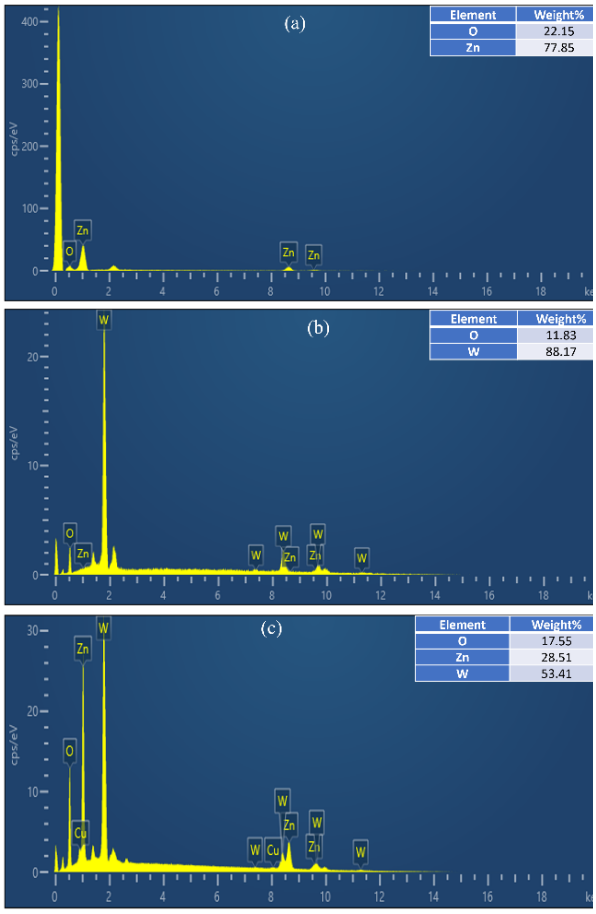

Figure 4. EDS spectrum of a) 100ZnO, b) 100WO_3, and (c) 50WO_3-50ZnO samples.

3.3. FT-IR analysis

The FT-IR spectra of 100ZnO, 100WO3, and 50WO3-50ZnO are shown in Figure 5. The significant peaks of the 100ZnO sample are located at 445 and 3448 cm^{-1}. The absorption band at 3448 cm^{-1} is attributed to the bending and stretching vibrational modes of water (-OH groups) molecules adsorbed on the surface of the samples. The peak at 445 cm^{-1} is associated with the stretching vibration of the Zn–O bond (Ying et al., 2019; Yu et al., 2011). The characteristic peaks of 100WO3 are observed at 771, 825, and 3448 cm^{-1}. The peak near 771 cm^{-1} is attributed to the stretching vibrations of W–O bonds, while the peak around 825 cm^{-1} corresponds to the asymmetric vibrations of W–O. Additionally, a smaller peak observed at approximately 1680 cm^{-1} is associated with the stretching vibrations of the W=O bonds (Aziz et al., 2023; Li et al., 2024). In the 50WO3-50ZnO sample, the characteristic peak of ZnO is noted at 445 cm^{-1}. As the content of WO3 increases and the amount of ZnO decreases, the intensity of this peak is reduced compared to the 100ZnO sample.

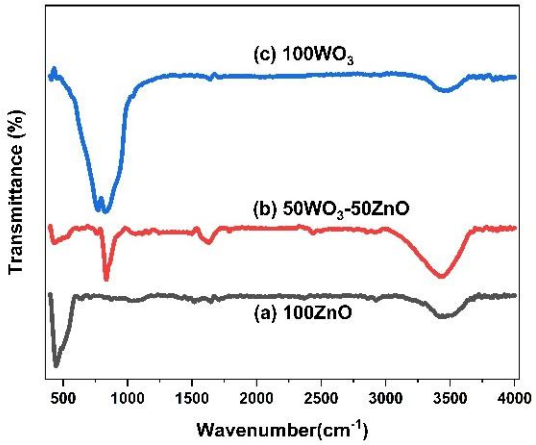

Figure 5. FT-IR analysis of (a) 100ZnO, (b) 50WO_3-50ZnO, and (c) 100WO_3.

3.4. Optical study

The optical properties of the synthesized 100ZnO, 100WO3, and 50WO3-50ZnO samples were examined using UV–Vis diffuse reflectance spectroscopy (DRS). The light absorption characteristics of the samples are depicted in Figure 6. As illustrated in Figure 6a, pure ZnO exhibits significant light absorption in the range of 200 to 380 nm, while showing minimal absorption in the visible light spectrum. Conversely, the 50WO3-50ZnO sample shows a blueshift in the absorption edge within the visible light range compared to pure 100ZnO, indicating that the presence of WO3 induces a shift of absorption towards shorter wavelengths.

These results suggest that the improved light absorption, associated with electron excitation from the valence band to the conduction band, is due to the shift of the absorption edge of the ZnO–WO3 nanocomposite into the visible spectrum (Lam et al., 2015). This shift enhances the movement of photogenerated electrons and holes (Wang et al., 2016; Xu & Chen, 2023). In addition, the pronounced reflectance observed in the visible light region highlights the potential of these composites for facilitating the photodegradation of pollutants (Lei et al., 2019).

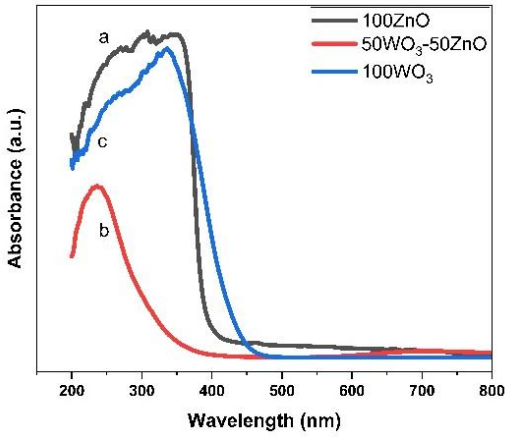

Figure 6. DRS analysis of (a) 100ZnO, (b) $50WO_3$-50ZnO, and (c) $100WO_3$.

The band gap energy of the as-synthesized samples was calculated by the Kubelka-Munk equation $(F(R)=(1-R)^2/2R)$, where R is the reflectance (Subash & Sasikala, 2025). The band gaps of the samples were determined from the plot of $(h\upsilon F(R))^n$ vs $E=h\upsilon$, assuming that the absorption coefficient is proportional to the KM function $(h\upsilon F(R))^n$. The constant value n is related to the direct (n=2) or indirect (n=0.5) band gap (Jafarabadi et al., 2023). The band gaps were achieved by extrapolating the linear part of the KM curve along with horizontal axis ($E=h\upsilon$). The optical direct band gap values of pure ZnO, pure WO_3, and $50WO_3$-50ZnO composites were estimated approximately to be 4.20, 3.03, and 3.29 eV, respectively (Figure 7).

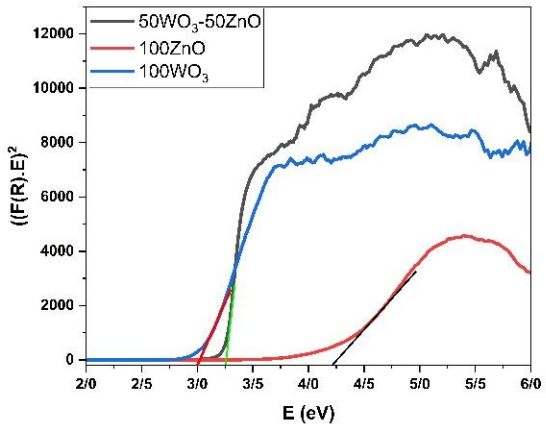

Figure 7. Kubelka-Munk transfaorm of DRS data for band gap of 100ZnO, $100WO_3$, and $50WO_3$-50ZnO samples.

These findings suggest that the integration of the ZnO and WO_3 semiconductor materials into a ZnO-WO_3 composite has the potential to alter the forbidden band width of the composite and enhance its optical absorption capabilities within the visible light spectrum (Xu & Chen, 2023). Consequently, the resultant heterostructure of ZnO-WO_3 composite enables the facilitation of electron transitions into conduction band of ZnO, thereby augmenting the light absorption efficiency of ZnO (Xu & Chen, 2023).

3.5. Photocatalytic degradation

The light absorption results of MO solution degradation under different durations of light irradiation and dark conditions in the presence of 100ZnO, 100WO3, and 50WO3-50ZnO are shown in Figure 8. The 50WO3-50ZnO photocatalyst exhibits superior photocatalytic efficacy compared to pure WO3 and ZnO. The change in absorbance of methyl orange (MO) for the 50WO3-50ZnO composite indicates that, as the irradiation time increases, the intensity of the maximum absorption peak at approximately 460 nm progressively decreases, ultimately becoming negligible after 15 minutes of irradiation. This observation demonstrates that the ZnO–WO3 composite can effectively degrade the MO solution. Consequently, the integration of ZnO with WO3 has the potential to enhance both visible light absorption and the photocatalytic performance of the individual components.

Previous studies have investigated the impact of incorporating WO3 into ZnO on surface characteristics and the efficiency of electron–hole pair separation. The findings indicate that even a small amount of WO3 can significantly improve the photocatalytic efficacy of ZnO in degrading various contaminants, including acid orange II (Yu et al., 2011), brilliant blue dye (Hunge et al., 2018), azo dyes (Chaudhary et al., 2020; Hindryawati et al., 2023; Lei et al., 2019), rhodamineB (Aziz et al., 2023), phthalic acid (Hunge et al., 2017), diclofenac (E et al., 2019), bisphenol A (Lam et al., 2013; Mokhtar et al., 2023; Rani et al., 2024), orange G (Adhikari et al., 2015), benzimidazoles (Li et al., 2024), auramine O (Rani et al., 2024), and oxytetracycline (Zhang et al., 2022). These studies reveal that the valence and conduction bands of WO3 exhibit more positive potentials compared to those of ZnO. As a result, the conduction band of WO3 acts as an electron sink, attracting photogenerated electrons from the conduction band of ZnO. Simultaneously, the valence band of ZnO functions as a hole acceptor, facilitating the transfer of holes from the valence band of WO3 to that of ZnO. This spatial separation of electron–hole pairs prolongs their lifetime and enhances overall photocatalytic performance (Hunge et al., 2017). The photogenerated holes interact with surface hydroxyl groups on the photocatalyst, forming hydroxyl radicals (Zhang et al., 2011), while the electrons reduce oxygen to generate superoxide radicals. These reactive species either directly attack the dye molecules or further generate hydroxyl radicals, which are ultimately responsible for the degradation of the pollutant. Based on the literature reports (Aziz et al., 2023; Faris et al., 2023), the suggested mechanism for the photocatalytic elimination of methyl orange is outlined as follows:

$WO_3/ZnO + h\upsilon \rightarrow h\upsilon WO_3/ZnO\ (e^-_{CB} + h^+_{VB})$
$WO_3/ZnO\ (e^-) + O_2 \rightarrow \cdot O_2^-$
$WO_3/ZnO\ (h^+) + OH^- \rightarrow \cdot OH + WO_3/ZnO$
$\cdot O_2^- + H_2O \rightarrow \cdot OOH + OH^- \rightarrow H_2O_2$
$H_2O_2 + \cdot O_2^- \rightarrow \cdot OH + OH^-$
$Dye + \cdot OH + \cdot O_2 \rightarrow$ Degradation products

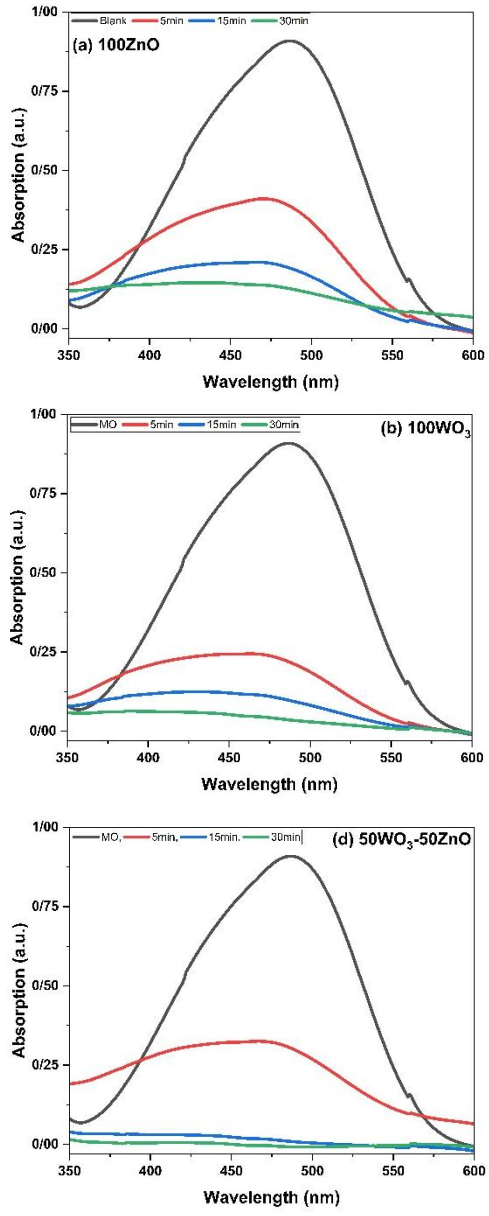

Figure 8. UV-Vis result of the MO degradation at different times of the light and dark conditions in the presence of (a) 100ZnO, (b) $100WO_3$, and (c) $50WO_3$-50ZnO samples.

4. CONCLUSION

ZnO, WO3, and the ZnO–WO3 composite were successfully prepared using a green synthesis method. The morphological, structural, and optical properties were characterized by FESEM, XRD, and UV–Vis absorption spectroscopy. Compared with pure ZnO and WO3, the ZnO–WO3 (50WO3-50ZnO) composite exhibited higher photocatalytic activity under UV–Vis light, as the presence of WO3 enhances the optical absorption of ZnO from the ultraviolet to the visible light region and inhibits the recombination of photo-induced charge carriers. The 50WO3-50ZnO composite achieved 100% dye removal within 15 minutes for methyl orange, demonstrating significantly superior performance compared to pure ZnO and WO3.

ACKNOWLEDGEMENTS

The Authors sincerely appreciate the Semnan University for the all supports throughout this work.

REFERENCES

1. Adhikari, S., Sarkar, D., & Madras, G. (2015). Highly efficient WO_3-ZnO mixed oxides for photocatalysis. *RSC Advances*, *5*. https://doi.org/10.1039/c4ra13210f
2. Alam, R., Hossain, M. A., & Elias, M. (2024). Amine functionalized graphene oxide decorated with ZnO-WO_3 nanocomposites for remediation of organic dye from wastewater. *Journal of Physics and Chemistry of Solids*, *190*, 112015. https://doi.org/10.1016/j.jpcs.2024.112015
3. Aziz, F., Warsi, A.-Z., Somaily, H. H., Din, M. I., Sabeeh, H., Warsi, M. F., & Shakir, I. (2023). Zinc oxide-tungsten oxide (ZnO-WO_3) composite for solar light-assisted degradation of organic dyes. *Korean Journal of Chemical Engineering*, *40*(6), 1497-1509. https://doi.org/10.1007/s11814-022-1368-9
4. Chaudhary, K., Shaheen, N., Zulfiqar, S., Sarwar, M. I., Suleman, M., Agboola, P. O., Shakir, I., & Warsi, M. F. (2020). Binary WO_3-ZnO nanostructures supported rGO ternary nanocomposite for visible light driven photocatalytic degradation of methylene blue. *Synthetic Metals*, *269*, 116526. https://doi.org/10.1016/j.synthmet.2020.116526
5. E, M., M.B, S., & P.E, J. (2019). Photocatalytic activity of ZnO-WO_3 for diclofenac degradation under visible light irradiation. *Journal of Photochemistry and Photobiology A: Chemistry*, *383*, 11199. https://doi.org/10.1016/j.jphotochem.2019.111993
6. Faris, A. H., Hamid, K. J., Naji, A. M., Mohammed, M. K. A., Nief, O. A., & Jabir, M. S. (2023). Novel Mo-doped WO_3/ZnO nanocomposites loaded with polyvinyl alcohol towards efficient visible-light-driven photodegradation of methyl orange. *Materials Letters*, *334*, 133746. https://doi.org/10.1016/j.matlet.2022.133746
7. Hamrouni, A., Lachheb, H., & Houas, A. (2013). Synthesis, characterization and photocatalytic activity of ZnO-SnO_2 nanocomposites. *Materials Science and Engineering: B*, *178*(20), 1371-1379. https://doi.org/10.1016/j.mseb.2013.08.008
8. Hindryawati, N., Ramadhani, W., Wirawan, T., & Maniam, G. P. (2023). Sonocatalytic degradation of methylene blue using WO_3-ZnO composite. *AIP Conference Proceedings*, *2431*(1), 050004. https://doi.org/10.1063/5.0115100
9. Hunge, Y. M., Mahadik, M. A., Moholkar, A. V., & Bhosale, C. H. (2017). Photoelectrocatalytic degradation of phthalic acid using spray deposited stratified WO_3/ZnO thin films under sunlight illumination. *Applied Surface Science*, *420*, 764-772. https://doi.org/10.1016/j.apsusc.2017.05.221
10. Hunge, Y. M., Yadav, A. A., & Mathe, V. L. (2018). Ultrasound assisted synthesis of WO_3-ZnO nanocomposites for brilliant blue dye degradation. *Ultrasonics Sonochemistry*, *45*, 116-122. https://doi.org/10.1016/j.ultsonch.2018.02.052

11. Jafarabadi, A., Sobhani, M., & Koohestani, H. (2023). Fabrication and characterization of highly visible-light responsive TiO_2/Fe_2TiO_5 ceramic. *Inorganic Chemistry Communications*, *154*, 111008. https://doi.org/10.1016/j.inoche.2023.111008

12. Lam, S.-M., Sin, J.-C., Abdullah, A. Z., & Mohamed, A. R. (2013). Sunlight photocatalytic activity enhancement of WO3/ZnO nanorod composites for degradation of bisphenol A *Chemeca 2013: Challenging Tomorrow, Barton, ACT*. https://search.informit.org/doi/10.3316/informit.882385542452534

13. Lam, S. M., Sin, J. C., Abdullah, A. Z., & Mohamed, A. R. (2015). Sunlight responsive WO_3/ZnO nanorods for photocatalytic degradation and mineralization of chlorinated phenoxyacetic acid herbicides in water. *J Colloid Interface Sci*, *450*, 34-44. https://doi.org/10.1016/j.jcis.2015.02.075

14. Lei, R., Zhang, H., Ni, H., Chen, R., Gu, H., & Zhang, B. (2019). Novel ZnO nanoparticles modified WO_3 nanosheet arrays for enhanced photocatalytic properties under solar light illumination. *Applied Surface Science*, *463*, 363-373. https://doi.org/10.1016/j.apsusc.2018.08.218

15. Li, N., Hu, Z., Li, Y., Zhou, R., Lan, G., & Gong, X. (2024). WO_3-ZnO as an anti-gastric cancer agent and efficient photocatalyst in the synthesis of substituted benzimidazoles. *Inorganic Chemistry Communications*, *161*, 112025. https://doi.org/10.1016/j.inoche.2024.112025

16. Liu, Z.-L., Deng, J.-C., Deng, J.-J., & Liu, F.-f. (2008). Fabrication and photocatalysis of CuO/ZnO nano-composites via a new method. *Materials Science and Engineering: B*, *150*, 99-104. https://doi.org/10.1016/j.mseb.2008.04.002

17. Mohammed, M. K. A., Ahmed, D. S., & Singh, S. (2022). Efficient and stable perovskite solar cells using the tungsten trioxide as an interfacial passivation layer. *Materials Letters*, *310*, 131518. https://doi.org/10.1016/j.matlet.2021.131518

18. Mokhtar, H., Mohd Hir, Z. A., Rafaie, H., & Ramli, N. (2023). Photodegradation of Bisphenol A using WO_3/ZnO Photocatalyst under Visible Light Irradiation. *Bioresources and Environment*, *1*, 54-64. https://doi.org/10.24191/bioenv.v1i3.45

19. Moradi, S., Aberoomand-Azar, P., Raeis-Farshid, S., Abedini-Khorrami, S., & Givianrad, M. H. (2016). The effect of different molar ratios of ZnO on characterization and photocatalytic activity of TiO_2/ZnO nanocomposite. *Journal of Saudi Chemical Society*, *20*(4), 373-378. https://doi.org/10.1016/j.jscs.2012.08.002

20. Nandiyanto, A., Zaen, R., & Oktiani, R. (2017). Correlation between crystallite size and photocatalytic performance of micrometer-sized Monoclinic WO_3 particles. *Arabian Journal of Chemistry*, *13*. https://doi.org/10.1016/j.arabjc.2017.10.010

21. Pei, C., & Leung, W. (2011). Photocatalytic degradation of Rhodamine B by TiO_2/ZnO nanofibers under visible-light irradiation. *Separation and Purification Technology*, *114*, 108–116. https://doi.org/10.1016/j.seppur.2013.04.032

22. Rani, M., Keshu, Pandey, S., Rishabh, Sharma, S., & Shanker, U. (2024). Sunlight assisted highly efficient photocatalytic remediation of organic pollutants by green biosynthesized ZnO@WO_3 nanocomposite. *Journal of Photochemistry and Photobiology A: Chemistry*, *446*, 115160. https://doi.org/10.1016/j.jphotochem.2023.115160

23. Saravanan, R., Karthikeyan, S., Gupta, V. K., Sekaran, G., Narayanan, V., & Stephen, A. (2013). Enhanced photocatalytic activity of ZnO/CuO nanocomposite for the degradation of textile dye on visible light illumination. *Materials Science and Engineering: C*, *33*(1), 91-98. https://doi.org/10.1016/j.msec.2012.08.011

24. Subash, B., & Sasikala, R. (2025). High-performance photocatalytic and antibacterial properties of WO3/ZnO honeycomb structures: synthesis and mechanistic insights. *Journal of the Iranian Chemical Society*, *22*(4), 849-869. https://doi.org/10.1007/s13738-025-03190-3

25. Wang, F., Jin, Z., Jiang, Y., Backus, E. H. G., Bonn, M., Lou, S. N., Turchinovich, D., & Amal, R. (2016). Probing the charge separation process on In_2S_3/Pt-TiO_2 nanocomposites for boosted visible-light photocatalytic hydrogen production. *Applied Catalysis B: Environmental*, *198*, 25-31. https://doi.org/10.1016/j.apcatb.2016.05.048

26. Xie, J., Zhou, Z., Lian, Y., Hao, Y., Liu, X., Li, M., & Wei, Y. (2014). Simple preparation of WO_3–ZnO composites with UV–Vis photocatalytic activity and energy storage ability. *Ceramics International*, *40*(8, Part A), 12519-12524. https://doi.org/10.1016/j.ceramint.2014.04.106

27. Xu, Y., & Chen, T. (2023). Development of nanostructured based ZnO@WO_3 photocatalyst and its photocatalytic and electrochemical properties: Degradation of Rhodamine B. *International Journal of Electrochemical Science*, *18*(4), 100055. https://doi.org/10.1016/j.ijoes.2023.100055

28. Yan, W., Fan, H., & Yang, C. (2011). Ultra-fast synthesis and enhanced photocatalytic properties of alpha-Fe_2O_3/ZnO core-shell structure. *Materials Letters - MATER LETT*, *65*, 1595-1597. https://doi.org/10.1016/j.matlet.2011.03.026

29. Ying, Y. L., Pung, S. Y., Sreekantan, S., Yee, Y. F., Ong, M. T., & Pung, Y. F. (2019). Structural and Antibacterial Properties of WO_3/ZnO Hybrid Particles against Pathogenic Bacteria. *Materials Today: Proceedings*, *17*, 1008-1017. https://doi.org/10.1016/j.matpr.2019.06.500

30. Yu, C., Yang, K., Shu, Q., Yu, J. C., Cao, F., & Li, X. (2011). Preparation of WO_3/ZnO Composite Photocatalyst and Its Photocatalytic Performance. *Chinese Journal of Catalysis*, *32*(3), 555-565. https://doi.org/10.1016/S1872-2067(10)60212-4

31. Zhang, D., Liu, Z., & Mou, R. (2022). Preparation and characterization of WO_3/ZnO composite photocatalyst and its application for degradation of oxytetracycline in aqueous solution. *Inorganic Chemistry Communications*, *142*, 109667. https://doi.org/10.1016/j.inoche.2022.109667

32. Zhang, J., Li, L., Yan, T., & Li, G. (2011). Selective Pt Deposition onto the Face (110) of TiO_2 Assembled Microspheres That Substantially Enhances the Photocatalytic Properties. *The Journal of Physical Chemistry C*, *115*(28), 13820-13828. https://doi.org/10.1021/jp203511z

33. Zheng, L., Zheng, Y., Chen, C., Zhan, Y., Lin, X., Zheng, Q., Wei, K., & Zhu, J. (2009). Network Structured SnO_2/ZnO Heterojunction Nanocatalyst with High Photocatalytic Activity. *Inorganic Chemistry*, *48*(5), 1819-1825. https://doi.org/10.1021/ic802293p